Intensity and wavelength control of a single molecule reaction: Simulation of photodissociation of cold-trapped MgH^+

Solvejg Jørgensen[a] and Michael Drewsen
Danish National Research Foundation Center for Quantum Optics, Department of Physics and Astronomy, University of Aarhus, DK-8000 Aarhus C, Denmark

Ronnie Kosloff
The Fritz Haber Research Center for Molecular Dynamics, Hebrew University, Jerusalem 91904, Israel

(Received 11 April 2005; accepted 11 July 2005; published online 2 September 2005)

Photodissociation of cold magnesium hydride ions MgH^+ leading to either Mg^++H or Mg+H^+ is simulated from first principles. The purpose is to study the possibility of single molecule control of the products in the presence of two laser fields. The system evolves on four electronic potential-energy curves, $X^1\Sigma$, $A^1\Sigma$, $B^1\Pi$, and $C^1\Sigma$. These potential-energy curves are calculated from first principles using multireference self-consistent field theory. The accuracy of the electronic potential curves has been checked by calculating the energies of the rovibrational eigenstates and comparing them to experimental findings. The photodissociation dynamics has furthermore been simulated by solving the time-dependent Schrödinger equation. It is shown that the branching ratio of the two dissociation channels, Mg^++H or Mg+H^+, can be controlled by changing the intensity and wavelength of the two driving laser fields. © *2005 American Institute of Physics*.
[DOI: 10.1063/1.2011398]

I. INTRODUCTION

An ultimate goal for coherent control of a chemical reaction is to apply the method on a single molecule level. The principle of coherent control is based on constructive quantum interference in the desired product channel and destructive interferences in all other product channels. Shaping of the light field and inducing the coherence to the matter waves are the current approaches to coherent control of the chemical reaction.[1,2] An optimal controllability of the photoreaction requires pulse shaping of the phase, the amplitude, and the polarization of the light field. A more simple approach for controlling the outcome is to tune the frequency and the intensity of the excitation to different excited electronic potential-energy surfaces which correlate to different asymptotic dissociation channels.

At the experimental level, only few observations of a chemical reaction of a single molecule have been reported.[3–6] A challenging objective is to control such a reaction. A prerequisite for this single molecule encounter is to localize/immobilize the reactants. In addition, the reaction products have to be stabilized in order to eliminate the back reaction. Two different experimental approaches have so far been employed. One is based on a surface-mediated reaction[3,4] whereas in the other approach a cold atomic ion in a so-called Coulomb crystal reacts with a molecular gas.[5,6]

In one of the surface experiments, Hahn and Ho[3] studied the formation of carbon dioxide CO_2 by catalytic oxidation of carbon monoxide on a Ag(110) surface. First, a scanning tunneling microscope (STM) tip was used to dissociate an oxygen molecule. Subsequently, a chemisorbed oxygen atom recombined with a chemisorbed carbon monoxide to form carbon dioxide. The product is stabilized by dissipating its excess energy to the surface. Control in such a surface-mediated experiment is limited. Only the energy of the electron can be varied, and therefore, there is no direct control of quantum interferences. Nevertheless, even this limited control has been shown to lead to selective excitation of a chemical bond.[7]

In the Coulomb crystal experiments, individual Ca^+ ions, which are excited due to the laser cooling process,[8] were observed to react with ambient oxygen gas to form CaO^+ molecular ions.[5] The molecular ions were translationally cooled ($T<10$ mK) through Coulomb interactions with the remaining laser-cooled atomic ions and spatially extremely well localized ($\sim 10\ \mu m^3$). Since the achieved confinement allows a laser beam to be focused onto a single ion,[9] such sympathetically cooled molecular ions are suitable candidates for single molecular reaction studies. Furthermore, it has recently been proven that nondestructive identification of single molecular ions is possible through *in situ* mass spectrometry.[6]

The present theoretical study explores controlled photodissociation of a single magnesium hydride ion MgH^+ in the presence of two picosecond laser pulses. In a complementary experiment, prerequisites will be cooling and immobilizing the MgH^+ ions as have been demonstrated earlier.[10] The photodissociation pathways are suggested by the potential-energy curves of MgH^+. The most relevant four lowest-lying singlet spin potential-energy curves are shown in Fig. 1.

The purpose of the present theoretical study is to explore the control possibilities of manipulating the branching ratio of the photodissociation products. The control scheme is based on varying the intensity and the wavelength of the two

[a]Electronic mail: solvejg@phys.au.dk

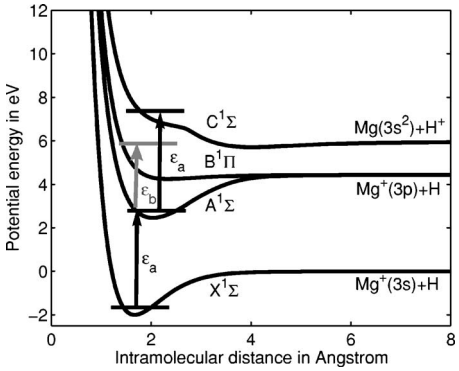

FIG. 1. The potential-energy curves for the four lowest-lying singlet spin electronic states of MgH^+. The potential-energy curves are computed by CBS(DTQ) extrapolation from the *ab initio* calculated potential energies. The computational details are given in the text. The symbols ϵ_a and ϵ_b represent the electric fields of the laser fields used in the photodissociation study.

laser pulses focusing onto a molecular ion localized in a string of ions. In order to carry out the study accurate potential-energy surfaces have to be established including the transition dipole moments. In addition the photodynamics has to be solved from the reactants to products under varying pulse conditions.

At a macroscopic level, we have studied the photodissociation reaction with a nanosecond laser.[11,12] This experiment follows the excitation scheme proposed for the single molecule experiment. We have shown that in the current experiment the rotational degree of freedom of the MgH^+ ions are only weakly sympathetically cooled by the surrounding laser-cooled Mg^+. The present study assumes rotationally cold MgH^+ ions. Schemes to further cool the MgH^+ molecular ion are under inversitigation.[13–15]

The scheme for the photodissociation process is presented in Sec. II. The adiabatic framework is used for our theoretical model described in Sec. III. Here, we compute the adiabatic potential-energy curves for the four relevant electronic states and the electronic dipole transition moments. The accuracy of the electronic potential-energy curves will be discussed. The dynamics of the photodissociation is visualized by solving the time-dependent Schrödinger equation. In Sec. IV the branching ratio between the two dissociation channels are computed as a function of the intensities and the wavelengths of the laser pulses. The conclusion and a general outlook are presented in Sec. V.

II. THE PHOTODISSOCIATION SCHEME OF MgH^+

The magnesium hydride ion MgH^+ is formed by a photochemical reaction, where a hydrogen gas reacts with laser-cooled magnesium ions in a Coulomb crystal.[5,8,11,16] In this case the MgH^+ ions are first formed in the electronic excited state $A^1\Sigma$, then they relax to the electronic ground state $X^1\Sigma$ by spontaneous emission. In this state, the magnesium hydride molecules relax to the lowest vibrational state due to the interactions with the blackbody radiation background in the trap region. At the present experimental conditions some rotational excitations still exist. The rotational temperature has been estimated to be above 120 K.[12] Additional schemes for rotational cooling of MgH^+ have been proposed by Vogelius *et al.*[13–15] The translational degrees of freedom of the molecular ions are sympathetically cooled by the Coulomb interactions with the remaining laser-cooled magnesium ions in the trap. Taking into account the prospect of rotational cooling, the initial state of the reactant MgH^+ in this photodissociation study is in the lowest internal state of the ground electronic state $X^1\Sigma$, e.g., $\nu=0$ and $J=0$.

The scheme for the photodissociation is shown in Fig. 1. The fields of these two picosecond laser pulses are denoted by ϵ_a and ϵ_b. The laser pulse ϵ_a, with frequency $\hbar\omega_a$, excites the molecular ion from the ground electronic state $X^1\Sigma$ to the first excited state $A^1\Sigma$,

$$\mathrm{MgH}^+(X^1\Sigma) + \hbar\omega_a \rightarrow \mathrm{MgH}^+(A^1\Sigma). \tag{1}$$

The wavelength of the electric field, ϵ_a, is tuned to the different initial electronic transitions. The lifetime of the excited MgH^+ in the $A^1\Sigma$ electronic state is 4.4 ns, since we consider the photodissociation of the MgH^+ ions with picosecond laser pulses, the spontaneous decay from $A^1\Sigma$ to $X^1\Sigma$ can be ignored. From the $A^1\Sigma$ state the MgH^+ ion has two excitation possibilities to either the $C^1\Sigma$ state by pulse ϵ_a or $B^1\Pi$ state by pulse ϵ_b,

$$\mathrm{MgH}^+(A^1\Sigma) + \hbar\omega_a \rightarrow \mathrm{MgH}^+(C^1\Sigma) \rightarrow \mathrm{Mg}(3s^2) + H^+, \tag{2}$$

$$\mathrm{MgH}^+(A^1\Sigma) + \hbar\omega_b \rightarrow \mathrm{MgH}^+(B^1\Pi) \rightarrow \mathrm{Mg}^+(3p) + H. \tag{3}$$

The two channels, $C^1\Sigma$ and $B^1\Pi$, correlate to different reaction products, $Mg(3s^2)+H^+$ and $Mg^+(3p)+H$, respectively. Experimentally, these products are detected by observing the changes in the resonant fluorescence of Mg^+ ions.[8,11,16] In the Mg^++H reaction product, the newly formed magnesium ion is trapped and starts fluorescing due to the interaction with the cooling laser field. In the other dissociation channel the H^+ ion escapes the trap.

The electric field of the laser pulse is described as

$$\epsilon_j(t) = \tfrac{1}{2}\bar{\epsilon}_j f_j(t)(e^{-i\omega_j t} + e^{i\omega_j t}), \quad \text{where } j = a,b, \tag{4}$$

where the amplitude involves a Gaussian envelope, $f_j(t) = \exp(-2\ln 2[(t-t_{p,j})/\tau_{c,j}]^2)$, centered at $t=t_{p,j}$ with the temporal width $\tau_{c,j}$, which is defined as the full width at half maximum (FWHM). The frequency is denoted by ω_j and $\bar{\epsilon}_j$ is the electric-field amplitude. The electric-field amplitude is related to the intensity of the laser $I=\frac{1}{2}\epsilon_0 c|\bar{\epsilon}|^2$, where c is the velocity of the light and ϵ_0 is the permittivity of vacuum. The intensity and the wavelength for each laser pulse are the control knobs $(I_a, I_b, \lambda_a, \lambda_b)$ of the dissociation branching ratio.

III. THE THEORETICAL MODEL

The molecular system is composed of N_e electrons and N_n nuclei. The electrons and the nuclei are located at $\boldsymbol{r}_e = (\boldsymbol{r}_{e,1}, \boldsymbol{r}_{e,2}, \ldots, \boldsymbol{r}_{e,N_e})$ and $\boldsymbol{r}_n = (\boldsymbol{r}_{n,1}, \boldsymbol{r}_{n,2}, \ldots, \boldsymbol{r}_{n,N_n})$, respectively. The dynamics of a light-driven molecular system is described by the time-dependent Schrödinger equation,

$$i\hbar\frac{\partial\Psi(\boldsymbol{r}_e,\boldsymbol{r}_n,t)}{\partial t}=\boldsymbol{H}(\boldsymbol{r}_e,\boldsymbol{r}_n,t)\Psi(\boldsymbol{r}_e,\boldsymbol{r}_n,t), \tag{5}$$

where the time-dependent Hamiltonian operator includes the interaction between the dipole operator of the molecular system $\hat{\boldsymbol{\mu}}$ and a time-dependent electric field $\boldsymbol{\epsilon}(t)$,

$$\hat{\boldsymbol{H}}(\boldsymbol{r}_e,\boldsymbol{r}_n,t)=\hat{\boldsymbol{H}}(\boldsymbol{r}_e,\boldsymbol{r}_n)+\boldsymbol{\epsilon}(t)\cdot\hat{\boldsymbol{\mu}}(\boldsymbol{r}_e,\boldsymbol{r}_n). \tag{6}$$

The stationary part of the hamiltonain $\hat{\boldsymbol{H}}(\boldsymbol{r}_e,\boldsymbol{r}_n)$ can be decomposed into nuclear and electronic parts to

$$\begin{aligned}\hat{\boldsymbol{H}}(\boldsymbol{r}_e,\boldsymbol{r}_n)&=\hat{\boldsymbol{T}}_n(\boldsymbol{r}_n)+\hat{\boldsymbol{T}}_e(\boldsymbol{r}_e)+\hat{\boldsymbol{V}}_{\text{tot}}(\boldsymbol{r}_e,\boldsymbol{r}_n)\\&\equiv\hat{\boldsymbol{T}}_n(\boldsymbol{r}_n)+\hat{\boldsymbol{H}}_e(\boldsymbol{r}_e|\boldsymbol{r}_n),\end{aligned} \tag{7}$$

where $\hat{\boldsymbol{T}}_n(\boldsymbol{r}_n)$ and $\hat{\boldsymbol{T}}_e(\boldsymbol{r}_e)$ denote the kinetic energy of the nuclei and the electrons, respectively. The operator $\hat{\mathbf{V}}_{\text{tot}}$ describes the Coulombic potential energy of the molecular system. In the time-dependent adiabatic representation, the total wave function of the molecular system is expanded using the adiabatic basis functions

$$\Psi(\boldsymbol{r}_e,\boldsymbol{r}_n,t)=\sum_j\Phi_{e,j}(\boldsymbol{r}_e|\boldsymbol{r}_n)\chi_{n,j}(\boldsymbol{r}_n,t), \tag{8}$$

where the set of orthonormal adiabatic electronic states $\{\Phi_{e,j}(\boldsymbol{r}_e|\boldsymbol{r}_n)\}$ satisfies the electronic adiabatic stationary Schrödinger equation:

$$\hat{\boldsymbol{H}}_e(\boldsymbol{r}_e|\boldsymbol{r}_n)\Phi_{e,j}(\boldsymbol{r}_e|\boldsymbol{r}_n)=\varepsilon_j(\boldsymbol{r}_n)\Phi_{e,j}(\boldsymbol{r}_e|\boldsymbol{r}_n). \tag{9}$$

The eigenvalue ε_j are the adiabatic potential-energy surfaces.

Integrating out the electronic degrees of freedom, a closed set of equations for the nuclear dynamics is obtained,

$$\begin{aligned}i\hbar\frac{\partial\chi_{n,i}(r_n,t)}{\partial t}&=\sum_j(\hat{\boldsymbol{T}}_{n,ij}(\boldsymbol{r}_n)+\boldsymbol{\mu}_{ij}(\boldsymbol{r}_n))\chi_{n,j}(\boldsymbol{r}_n,t)\\&\quad+\varepsilon_i(\boldsymbol{r}_n)\chi_{n,i}(\boldsymbol{r}_n,t),\end{aligned} \tag{10}$$

where $\hat{\boldsymbol{T}}_{n,ij}(\boldsymbol{r}_n)=(\hat{\boldsymbol{T}}_n+\hat{\boldsymbol{A}}_{n,ij}(\boldsymbol{r}_n))^2$ and

$$\hat{\boldsymbol{A}}_{n,ij}(\boldsymbol{r}_n)=\langle\Phi_{e,i}(\boldsymbol{r}_e|\boldsymbol{r}_n)|\hat{\boldsymbol{T}}_n|\Phi_{e,j}(\boldsymbol{r}_e|\boldsymbol{r}_n)\rangle_{r_e}. \tag{11}$$

The symbol $\langle\cdots\rangle_{r_e}$ indicates that the integration is done over the electronic domain. The electronic transition dipole moments, which couple two adiabatic surfaces, are defined by

$$\hat{\boldsymbol{\mu}}_{ij}(\boldsymbol{r}_n)=\langle\Phi_{e,i}(\boldsymbol{r}_e|\boldsymbol{r}_n)|\hat{\boldsymbol{\mu}}(\boldsymbol{r}_e,\boldsymbol{r}_n)|\Phi_{e,j}(\boldsymbol{r}_e|\boldsymbol{r}_n)\rangle_{r_e}. \tag{12}$$

A. Time-independent adiabatic framework

The first step is to compute the electronic adiabatic potential-energy curves of MgH^+ by solving the adiabatic electronic Schrödinger equation given in Eq. (9). The bond length between the two atoms is defined as the distance between the two nuclei, e.g., $r=|\mathbf{r}_{\text{Mg}}-\mathbf{r}_{\text{H}}|$. For the energy scale of interest, the four lowest-lying singlet spin electronic states are of relevance. The accuracy of the simulation depends crucially on the accuracy of the adiabatic potential-energy curves. To estimate the accuracy of the potential-energy curves the calculated molecular rovibrational eigenenergies are compared to spectroscopic measurements carried out by Balfour.[17] Theoretically, this requires solving the adiabatic nuclear time-independent Schrödinger equation for the individual curves. In this calculation the off-diagonal coupling elements are neglected, e.g., $\hat{\boldsymbol{T}}_{n,ij}=0$ for $i\neq j$.

1. Adiabatic potential-energy curves

It is a challenging task to compute accurate electronic adiabatic potential-energy curves (PES). The accuracy of the adiabatic potential-energy curves depends on both the selection of the approximate solution of the electronic Schrödinger equation Eq. (9) and the choice of the basis set. For a given basis set the goal is to approach the full-configuration-interaction (FCI) limit. For ground-state adiabatic potential-energy curves this is possible with highly correlated methods such as multireference configuration interaction (MCRI) and coupled cluster, for example, CCSD(T). As the number of the basis function increases, the calculation effort explodes. To overcome this difficulty, a method to extrapolate the *ab initio* energy at the complete basis set (CBS) limit has been developed.[18–21] The PES is systematically computed with progressively larger basis sets, and the results are then extrapolated to infinity, e.g., to the complete basis set limit. The complete basis set extrapolation method had been used for many of different applications such as calculating thermodynamical properties,[22,23] adiabatic potential-energy surfaces/curves,[24,25] and geometry and frequency optimization.[19] All the above applications were of the ground-state properties. Here, the CBS scheme is also used for extrapolating the adiabatic potential-energy curves of the electronic excited states.

For a fixed nuclear coordinate configuration the adiabatic electronic potential energy at the complete basis limit is extrapolated by

$$\varepsilon_j(l)=E_{\text{CBS},j}+A(l+1/2)^{\alpha}, \tag{13}$$

where l is the maximum angular quantum number in the basis set and $\varepsilon_j(l)$ is the energy obtained form this basis set for the jth electronic state. Due to the nonlinearity of this equation the fitting is difficult. The equation can be approximated with integer exponents,

$$\varepsilon_j(l)=E_{\text{CBS},j}+A(l+1/2)^{-4}+B(l+1/2)^{-6} \tag{14}$$

or

$$\varepsilon_j(l)=E_{\text{CBS},j}+A(l+1/2)^{-4}. \tag{15}$$

The complete basis set limit ($E_{\text{CBS},j}$) for the jth electronic state can be estimated for the two formulas Eqs. (14) and (15).

The present calculations employ the series of correlation consistent polarized valence n-tripled zeta (cc-pVnZ) basis sets,[26,27] where n=D,T,Q. The maximum angular quantum number l is 2, 3, and 4, respectively. The diffuseness of the charge distribution of the hydrogen atom requires an augmented basis set, therefore, a series of aug-cc-pVnZ are used for the hydrogen atom. For Mg the cc-pVnZ functions are used, since the charge distribution is concentrated around the magnesium nuclei, an augmented basis function set is not

TABLE I. The energy differences relative to the ground electronic state at the dissociation limit are tabulated. The energies are given in eV.

Asymptote	Atomic energy	DZ	TZ	QZ
$Mg^+(3p)+H$	4.43	4.2844	4.2774	4.2775
$Mg(3s^2)+H^+$	5.9522	6.0864	6.1022	6.1079

expected to significantly improve the basis set convergence. The selection of a basis set will only be denoted by n. In this abbreviation CBS(DTQ) implies that *ab initio* energy points of the three basis have been extrapolated to the complete basis limit using Eq. (14) whereas CBS(DT), CBS(DQ), and CBS(TQ) indicate that the adiabatic potential-energy curves have been extrapolated by Eq. (15).

The adiabatic potential-energy calculations were obtained at the multiconfiguration self-consistent field (MCSCF) level (Refs. 28 and 29. The active space consists of the two valence electrons in five orbitals corresponding to $1s$ atomic orbital of the hydrogen atom as well as $3s$ and $3p$ atomic orbitals of the magnesium atom. The electronic calculations were performed in the reduced C_{2v} point-symmetry group. All calculations were preformed with the MOLPRO 2000 program package.[30] The adiabatic potential-energy curves were computed as a function of the bond length r, taking values from 1 to 25 bohrs for the four lowest-lying singlet spin electronic states, e.g., $X^1\Sigma$, $A^1\Sigma$, $B^1\Pi$, and $C^1\Sigma$.

For large intramolecular distances the molecular configuration is given by two noninteracting atomic systems (see Fig. 1). The energy difference between the different atomic states is experimentally known.[16] In Table I the energy differences at large bond length r are shown for the electronic states employing the three different basis sets. A comparison between the *ab initio* computed energies and the atomic energies shows that the deviation for the asymptotic state, $Mg^+(3p)+H$, is 3.5% almost independent of the basis sets. Whereas the asymptote, $Mg(3s^2)+H^+$, varies with the choice of the basis set and the deviation from the atomic energies is around 2%. The actual potential-energy curves used were shifted by a constant energy in order to match the experimental vertical shifts at the asymptotic atomic limit.

The CBS extrapolation was carried out on the ground electronic state as well as on the excited electronic states obtained by Eqs. (14) and (15).

2. Rovibrational states

The energies of the rovibrational states, $X^1\Sigma$ and $A^1\Sigma$, were computed using the adiabatic potential-energy curves. The wave function and its corresponding energy of the rovibrational state χ_{vJ} were obtained by solving the adiabatic nuclear time-independent Schrödinger equation. Neglecting the nonadiabatic coupling between the different electronic states the radial equation is obtained,

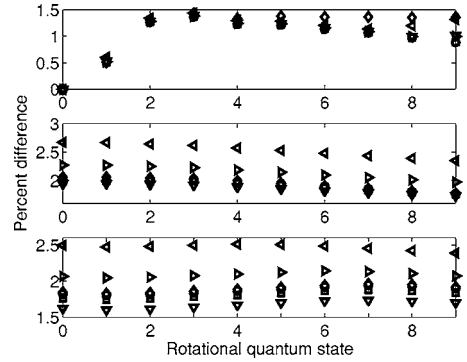

FIG. 2. The absolute percentage difference between the experimental rovibrational energy levels (Ref. 17 and the presented computed level for the ground electronic state $X^1\Sigma$ using different basis sets. The rovibrational energy for $E[X^1\Sigma(\nu=0,J=0)]=0$ for all the PES's. The upper panel shows the absolute deviation for the rotational states with $\nu=0$, the center with $\nu=1$, and the lower one with $\nu=2$. The left pointing triangles represent the TZ basis set, the right-pointing triangles represent the QZ basis set, the downward-pointing triangles represent the CBS(DT) extrapolation, the squares represent the CBS(DQ) extrapolation, the circles represent the CBS(TQ) extrapolation, and the diamonds represent the CBS(DTQ) extrapolation.

$$\boldsymbol{H}\chi_{\nu J}(r) = \left[-\frac{1}{2M_\mu}\frac{\partial^2}{\partial r^2} + \frac{J(J+1)}{2M_\mu r^2} + \boldsymbol{\varepsilon}(r)\right]\chi_{\nu J}(r) = E_{\nu J}\chi_{\nu J}(r). \tag{16}$$

The kinetic-energy operator of the nuclear motion has been decomposed into the radial kinetic energy and the azimuthal term. The numerical method for evaluating the eigenfunction is based on propagating a trial wave function on a discrete grid according to the time-dependent Schrödinger equation in the imaginary time.[31]

The computed eigenenergies of the rovibrational state were compared to the experimentally measured energies of Balfour.[17] Figures 2 and 3 show the absolute percentage difference between the experimental rovibrational energy re-

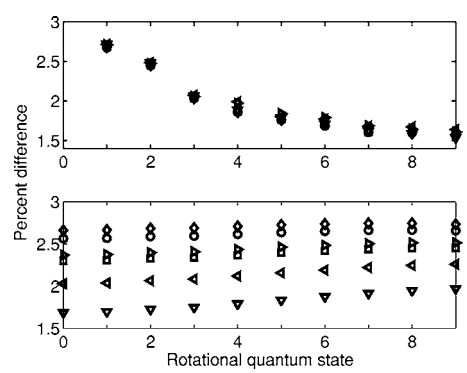

FIG. 3. The absolute percentage difference between the experimental rovibrational energy levels (Ref. 17 and the computed level for the electronic state $A^1\Sigma$ using different basis sets. The rovibrational energy has been compared relative to $E[A^1\Sigma(\nu=0,J=0)]$. The energies of $E[A^1\Sigma(\nu=0,J=0)]$ for the different computational methods are within a 2% from the experimentally observed. The upper panel shows the absolute deviation for the rotational states with $\nu=0$, and the lower one with $\nu=1$. The left-pointing triangles represent the TZ basis set, the right-pointing triangles represent the QZ basis set, the downward-pointing triangles represent the CBS(DT) extrapolation, the squares represent the CBS(DQ) extrapolation, the circles represent the CBS(TQ) extrapolation, and the diamonds represent the CBS(DTQ) extrapolation.

TABLE II. The computed rovibrational energy for CBS(DTQ) potentential-energy curve and the experimental values (Ref. 17 are compared. All the energies are given in cm^{-1}.

J	$\nu=0$ (This work)	$\nu=0$ (Ref. 17)	$\nu=1$ (This work)	$\nu=1$ (Ref. 17)
		$X^1\Sigma$		
0	0.00	0.0	1599.37	1634.36
1	12.47	12.49	1611.32	1646.70
2	37.26	37.74	1635.23	1671.11
3	74.49	75.56	1671.09	1707.90
4	124.13	125.75	1719.39	1756.62
5	186.08	188.60	1779.88	1817.61
6	260.28	263.81	1852.37	1890.62
7	346.76	351.48	1936.78	1975.78
8	445.39	451.43	2032.98	2072.87
9	556.16	563.73	2140.88	2181.88
		$A^1\Sigma$		
0	35 691.38	35 628.81	36 771.34	36 747.90
1	35 699.80	35 637.44	36 779.81	36 756.33
2	35 716.71	35 654.73	36 796.77	36 773.32
3	35 742.02	35 680.51	36 822.20	36 798.54
4	35 775.70	35 714.90	36 856.11	36 832.33
5	35 817.82	35 757.73	36 898.50	36 874.51
6	35 868.25	35 809.12	36 949.36	36 925.01
7	35 926.96	35 868.84	37 008.70	36 983.88
8	35 994.00	35 937.11	37 076.29	37 051.03
9	36 069.30	36 013.71	37 151.49	37 126.43

ported by Balfour[17] and the present calculation. In Table II the computed rovibrational energies for CBS(DTQ)-extrapolated potentential-energy curve are compared directly with the experimental values of Balfour (Ref. 17. For the ground state with the vibrational quanta $\nu=0$, small variations with respect to the type of the PES are observed. The CBS(TQ)-extrapolated adiabatic potential curve gives a slightly better agreement with the experimental result. For the vibrational excited states, $\nu=1$ and $\nu=2$, the accuracy is improved by using the CBS-extrapolated adiabatic potential-energy curves. The deviations in the rovibrational energies when the extrapolated adiabatic potentials are used was found to be less than 2%.

For the excited electronic state $A^1\Sigma$, the rovibrational energies have been compared relative to the energy of the lowest eigenstate in $A^1\Sigma$, e.g, $E[A^1\Sigma(\nu=0,J=0)]$. The energies of $E[A^1\Sigma(\nu=0,J=0)]$ for the different computational methods are within 2% of the experimental value. For the energies of the rovibrational states of the $A^1\Sigma$ state, a very small variation with respect to the type of the adiabatic potential for $\nu=0$ was observed but large variations were found for $\nu=1$ (cf. Fig. 3). For the ground vibrational state $\nu=0$, the CBS(TQ) gives the best agreement with the experimental observables whereas this extrapolated adiabatic potential is not satisfactory for $\nu=1$.

The adiabatic potential-energy curves for the ground state and the excited states have previously been computed.[32–35] The dissociation energies of the adiabatic potential-energy curves are compared with values in the literature (cf. Table III). For both the electronic ground state and the excited state there is good agreement with the adiabatic potentials and the values extracted from experimental observables.[35]

TABLE III. Experimentally derived values (Ref. 35) and computational estimations of the dissociation energies of MgH^+ for the three lowest-lying singlet spin electronic states. All the values are reported in eV.

Reference	$X^1\Sigma$	$A^1\Sigma$	$B^1\Pi$
Ref. 35 experiment	2.1	2.0	
Ref. 33 theory	2.03	1.95	0.20
Ref. 34 theory	1.93	1.93	0.18
Ref. 32 theory	1.78	1.75	0.169
DZ	1.899	1.915	0.155
TZ	1.982	1.968	0.182
QZ	1.995	1.972	0.185
CBS(DT)	2.010	1.986	0.192
CBS(DQ)	2.005	1.978	0.186
CBS(TQ)	2.003	1.975	0.187
CBS(DTQ)	2.002	1.974	0.187

Altogether, the accuracy is better than 3% for the adiabatic potential-energy curves of the ground state $X^1\Sigma$ and the lowest-lying singlet spin excited electronic state $A^1\Sigma$. The accuracy of the two other excited states is not known. In the dynamical simulation of the photodissociation the CBS(DQT)-extrapolated adiabatic potential curves have been used. The sensitivity of the branching ratio to the different extrapolations methods has been checked. The variations are found to be small (cf. Sec. IV).

3. Electronic transition dipole moment

The electronic transition dipole moment Eq. (12) is directly calculated by the electronic structure model. The transition dipole moments are shown in Fig. 4. The electronic dipole transition moments, μ_{XA} and μ_{AB}, show only small variations with respect to the choice of basis set. The dipole function for the $A^1\Sigma \rightarrow C^1\Sigma$ transition, $\mu_{AC}(r)$, was found to have a strong dependence on the selected basis set. Analyzing the CI coefficient of the electronic wave function of the $C^1\Sigma$ state around $r\sim 3$–6 Å shows that several of the states

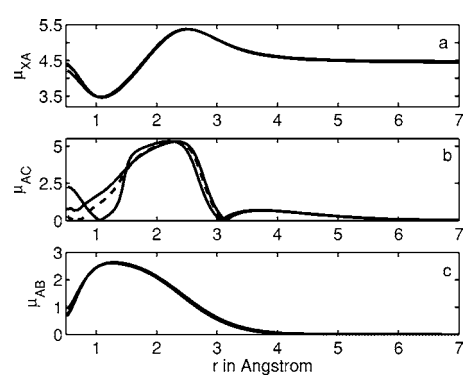

FIG. 4. The electronic transition dipole moments as a function of the intramolecular distance are shown for different electronic transitions in MgH^+ using different basis sets. The basis set DZ is displayed with a solid line, TZ basis set with a dashed line, and QZ basis set with a dashed-dotted line. (a) μ_{XA} represents the electronic dipole transition moment from $X^1\Sigma$ to $A^1\Sigma$ transition, (b) μ_{AC} represents the transition from $A^1\Sigma$ to $C^1\Sigma$, and (c) μ_{AB} represents the transition from $A^1\Sigma$ to $B^1\Pi$ transition.

contribute. These include the double occupation of the s and the p orbitals of the Mg atom. These observations can be rationalized by noticing that the charge is located on the hydrogen atom at the asymptote of the $C^1\Sigma$ state.

B. Time-dependent adiabatic framework

The dynamics of the photodissociation of MgH^+ is obtained by solving the time-dependent close-coupled equations Eq. (10). For the nuclear coordinate r they become

$$i\hbar\frac{\partial \boldsymbol{\chi}_i(r,t)}{\partial t} = \hat{\boldsymbol{H}}(r,t)\boldsymbol{\chi}_i(r,t) = [\boldsymbol{T}_n(r) + \varepsilon_i(r)]\boldsymbol{\chi}_i(r,t) + \sum_j \epsilon(t)\hat{\boldsymbol{\mu}}_{ij}\boldsymbol{\chi}_j(r,t), \tag{17}$$

where the off-diagonal adiabatic coupling elements of $T_{ij}(t)$ have been omitted. The wave function $\boldsymbol{\chi}$ represents the motion of the nuclei dynamics on the four relevant adiabatic potential-energy curves, and it is described as a state vector

$$\boldsymbol{\chi}(r,t) = \begin{pmatrix} \boldsymbol{\chi}_C(r,t) \\ \boldsymbol{\chi}_B(r,t) \\ \boldsymbol{\chi}_A(r,t) \\ \boldsymbol{\chi}_X(r,t) \end{pmatrix}. \tag{18}$$

The subscripts X, A, B, and C denote the electronic state $X^1\Sigma$, $A^1\Sigma$, $B^1\Pi$, and $C^1\Sigma$, respectively. Before the laser field is applied at time $t=t_{\text{start}}$ the MgH^+ ion is in the rovibrational state of the lowest electronic state. The wave function of the total system is represented by

$$\boldsymbol{\chi}(r,t=t_{\text{start}}) = \begin{pmatrix} 0 \\ 0 \\ 0 \\ \boldsymbol{\chi}_{\nu J}(r) \end{pmatrix}. \tag{19}$$

As described in Sec. II the molecular ion is in the lowest vibrational state due to the interaction with the blackbody radiation background in the trap region.[13] We assume that the molecular ion is in its lowest rotational state, e.g., $\nu=0$ and $J=0$.

The Hamiltonian is defined as

$$\boldsymbol{H}(r) = \begin{bmatrix} \boldsymbol{T}+\varepsilon_C(r) & 0 & \boldsymbol{\mu}_{CA}(r)\epsilon_a(t) & 0 \\ 0 & \boldsymbol{T}+\varepsilon_B(r) & \boldsymbol{\mu}_{BA}(r)\epsilon_b(t) & 0 \\ \boldsymbol{\mu}_{AC}(r)\epsilon_a(t) & \boldsymbol{\mu}_{AB}(r)\epsilon_b(t) & \boldsymbol{T}+\varepsilon_A(r) & \boldsymbol{\mu}_{AX}(r)\epsilon_a(t) \\ 0 & 0 & \boldsymbol{\mu}_{XA}(r)\epsilon_a(t) & \boldsymbol{T}+\varepsilon_X(r) \end{bmatrix}.$$

The diagonal elements are the channel Hamiltonians. The kinetic energy becomes $\boldsymbol{T}=-(1/2M_{mu})(\partial^2/\partial r^2)$. The terms $\varepsilon_i(r)$ are the adiabatic potential-energy curves. The four electronic curves are coupled by the interaction of the time-dependent laser field with the dipole moment operator. The laser field ϵ_a couples $X^1\Sigma$ and $A^1\Sigma$ as well as $A^1\Sigma$ with $C^1\Sigma$. The laser field ϵ_b couples the $A^1\Sigma$ state with $B^1\Pi$.

To avoid the fast oscillating frequency of the electric field [$e^{-i\omega t}$ in Eq. (4)], the rotating wave approximation has been employed.

Once the Hamiltonian and the initial state are initialized, the MgH^+ photodissociation is simulated by numerically integrating the time-dependent Schrödinger equation. The method is based on a grid representation of the wave function. The kinetic-energy operator has been evaluated by using the fast Fourier transformation technique.[36,37] Using small time steps, the Hamiltonian can be treated as time independent in each time step, the propagation in time is carried out using a Chebychev polynomial expansion of the evolution operator.[37] The computational parameters are summarized in Table IV. The total propagation time is 15 ps. At large intramolecular distances, $r \gg r_{\text{flux}}$, a complex exponential absorbing potential was used to impose outgoing boundary conditions.[38–40]

IV. RESULTS AND DISCUSSION

The analysis starts from the initial state $X^1\Sigma(\nu=0,J=0)$. At time $t_{\text{start}}=-7.5$ ps, the laser pulses, ϵ_a and ϵ_b, are initiated. The pulse ϵ_a excites the molecule from the $X^1\Sigma$ ground state and to the $A^1\Sigma$ excited state. Since the frequency of the excitation is below the threshold for dissociation of $A^1\Sigma$, the dissociation on this excited state is negligible. The pulse duration is 15 ps, since the lifetime of MgH^+ in $A^1\Sigma$ is 4.4 ns, the spontaneous decay from $A^1\Sigma$ to $X^1\Sigma$

TABLE IV. The typical values of the propagation parameters.

Parameters	Typical values	Units
Grid spacing δr	0.05	bohr
Number of grid points N_r	512	
Center of pulse $t_{p,a}$	0	ps
Temporal width $\tau_{c,a}$	3.5	ps
Center of pulse $t_{p,b}$	0	ps
Temporal width $\tau_{c,b}$	5.7	ps
Time steps δt	1.5	fs
Propagation initial time t_{start}	−7.5	ps
Propagation final time t_{stop}	7.5	ps
Order of the Chebychev polynomials	100	
Flux line r_{flux}	7	Å

can be ignored. Upon excitation to the $A^1\Sigma$ electronic state the molecule can further be excited to either the $C^1\Sigma$ state by the laser field ϵ_a or to $B^1\Pi$ with the laser field ϵ_b. From Fig. 1 it is clear that the $C^1\Sigma$ channel dissociates to $Mg^+(3p)+H$, whereas the $B^1\Pi$ channel dissociates to $Mg(3s^2)+H^+$. The branching ratio between the two dissociative channels are determined by integrating the flux of the dissociating wave packet at $r_{\text{flux}}=7$ Å on the individual potential-energy curves. (See Fig. 4.) The total accumulated flux of dissociating molecules in the kth channel is computed by

$$F_k = \sum_i^{N_t} J_k(t_i)\,\delta t = \frac{\delta t}{M_\mu}\sum_i^{N_t} \text{Im}\left[\chi_k^*(r_{\text{flux}},t_i) \times \left|\frac{\partial \chi_k(r,t_i)}{\partial r}\right|_{r=r_{\text{flux}}}\right], \tag{20}$$

where the derivative is evaluated with a Fourier transform.

Two control knobs for each of the two picosecond laser pulses can be manipulated; the intensities (I_a and I_b) and the wavelengths (λ_a and λ_b). All four knobs can be used to control the branching ratio between the two dissociative channels. The branching ratio is defined by

$$I = \frac{F_B(\text{Mg}^+(3p)+\text{H})}{F_B(\text{Mg}^+(3p)+\text{H}) + F_C(\text{Mg}(3s^2)+\text{H}^+)}, \tag{21}$$

when I approaches unity the product of the photodissociation reaction becomes $Mg^+(3p)+H$. For I approaching zero the reaction product would be $Mg(3s^2)+H^+$. Only small variations are observed in the branching ratio and accumulated flux when the CBS(DTQ)-extrapolated potential is changed with CBS(TQ), CBS(DQ), or CBS(DT).

A. Wavelength-controlled photodissociation

Direct insight into the influence of the frequencies of the fields on the dissociation branching ratio can be obtained by examining the detuning for the different electronic transitions,

$$\Delta_{AB} = \varepsilon_B - \varepsilon_A - \hbar\omega_b,$$
$$\Delta_{AC} = \varepsilon_C - \varepsilon_A - \hbar\omega_a, \tag{22}$$
$$\Delta_{XA} = \varepsilon_X - \varepsilon_A - \hbar\omega_a.$$

The detunings vary with the bond length. For the excitation wavelengths $\lambda_a=280$ nm and $\lambda_b=560$ nm, the detunings are shown as a function of the bond length r in Fig. 5. At the equilibrium position of the ground state $r_e\sim 1.66$ Å, the detuning $\Delta_{XA}=0$ is at resonance with the vertical electronic transition $X^1\Sigma$ to $A^1\Sigma$. For phase-locked wavelengths $\lambda_b=2\lambda_a$, the electronic transition $A^1\Sigma$ to $B^1\Pi$ is always off resonant.

Figure 6 shows the variation of the branching ratio and the accumulated fluxes as a function of the wavelength λ_a. We have scanned the wavelength from 270 to 281 nm, we found two minima in the branching ratio; one at 271.89 nm and another at 280.18 nm. They correspond to the resonant electronic transitions from $X^1\Sigma(\nu=0)$ to $A^1\Sigma(\nu=1)$ and

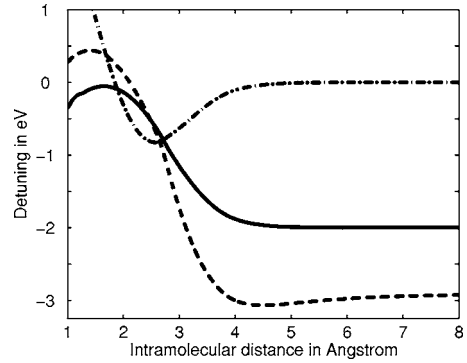

FIG. 5. The detunings of the laser fields are shown as a function of the bond length for $\lambda_a=280$ nm and $\lambda=560$ nm. The detunings Δ_{AB}, Δ_{AC}, and Δ_{XA} are marked with solid, dashed, and dotted-dashed lines, respectively.

$X^1\Sigma(\nu=0)$ to $A^1\Sigma(\nu=0)$, respectively. If the wavelength of the laser field ϵ_a is tuned to these two resonant wavelengths, then the yield in the dissociation channel, $Mg(3s^2)+H^+$, is strongly enhanced [cf. Fig. 6(b)]. For high intensity the probability for the product $Mg+H^+$ becomes 1 at the resonant wavelengths. For $\lambda_b=560$ nm the detuning Δ_{AB} for the electronic transition $A^1\Sigma$ to $B^1\Pi$ is always negative and off resonance. Only if the λ_a is off resonant the dissociating molecule can be directed into the $Mg^+(3p)+H$ channel. However, the probability for such a process is very small. As the wavelength λ_b increases the two dissociation channels start to compete. For a wavelength $\lambda_b=620$ nm $\Delta_{AB}\sim 0$ is at resonance at $r_e\sim 1.66$ Å, in this case the probability to exit in Mg^++H dissociation channel is about 7%.

In Figure 7 the branching ratio is shown as a function of the wavelength λ_b. As the wavelength of the laser increases two phenomena are observed: the detuning Δ_{AB} of the electronic transition from $A^1\Sigma$ and $B^1\Pi$ becomes resonant and the electronic transition changes from a bound-unbound to a bound-bound electronic transition. The threshold for dissociation is $\lambda_b\sim 630$ nm. The electronic transition from $A^1\Sigma$ and $B^1\Pi$ changes from a bound-unbound to a bound-bound electronic transition at $\lambda_b\sim 630$ nm. Around this wavelength

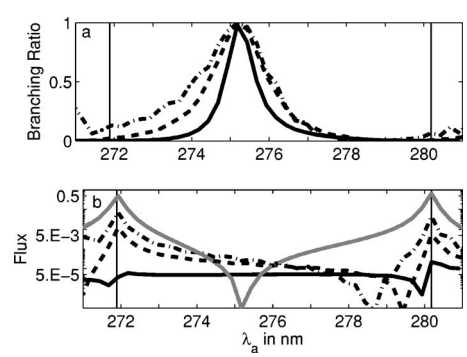

FIG. 6. (a) The branching ratio as a function of the wavelength λ_a given in nm. (b) The accumulated flux (log scale) as a function of the wavelength λ_a (in nm). The accumulated flux for the $Mg(3s^2)+H^+$ dissociation channel is shown with grey whereas the $Mg^+(3p)+H$ channel is indicated with black. Both the branching ratio and the accumulated flux are shown for three different wavelengths of λ_b given by $\lambda_b=2\lambda_a$ (solid line), $\lambda_b=590$ nm (dashed line), and $\lambda_b=620$ nm (dotted-dashed line). The intensities of the laser pulses are $I_a=I_b=1\times 10^9$ W/cm^2. The black vertical lines indicate the transition frequencies for the transitions $X^1\Sigma(\nu=0)$ to $A^1\Sigma(\nu=1)$ and $X^1\Sigma(\nu=0)$ to $A^1\Sigma(\nu=0)$, respectively.

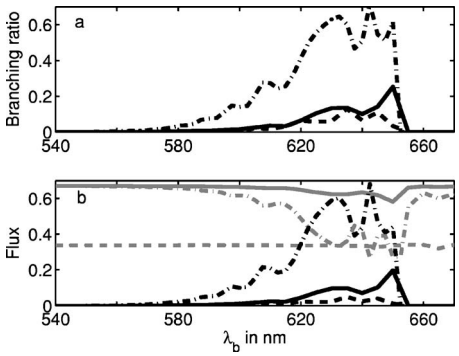

FIG. 7. (a) The branching ratio as a function of the wavelength λ_b given in nm. (b) The accumulated flux (log scale) as a function of the wavelength λ_b (in nm). The accumulated flux for the $Mg(3s^2)+H^+$ dissociation channel is indicated with grey whereas the $Mg^+(3p)+H$ channel is shown with black. In both figures the set of parameters are the following: $I_a=I_b=1\times10^9$ W/cm^2, $\lambda_a=280.89$ nm indicated with solid line, $I_a=I_b=1\times10^9$ W/cm^2, $\lambda_a=280.79$ nm indicated with dashed line, and $I_a=1\times10^9$ W/cm^2, $I_b=1\times10^{10}$ W/cm^2, $\lambda_a=280.89$ nm indicated with dot-dashed line.

the detuning $\Delta_{AB}=0$ around $r_e\sim1.66$ Å leading to an enhancement of the population transferred to the $B^1\Pi$ electronic state. If the intensity of the laser field ϵ_b is increased by a factor of 10 the $Mg^+(3p)+H$ dissociation channel dominates. Above the dissociation threshold part of the wave packet excited to the $B^1\Pi$ electronic state is bound, therefore, a certain fraction of the wave packet does not dissociate.

B. Intensity-controlled photodissociation

Figure 8 shows the branching ratio as a function of the intensities of the two laser pulses for two sets of wavelengths. It is clear that the intensities have a strong influence on the yields and therefore also on the branching ratio. In general, the relative yield of producing magnesium ions in the trap increases with the intensity I_b leading to large population transfer between $A^1\Sigma$ and $B^1\Pi$ electronic states. As the intensity I_a increases the coupling between the two electronic states, $A^1\Sigma$ and $C^1\Sigma$, increases leading to large yield in the $Mg(3s^2)+H^+$ dissociation channel. For the set, $\lambda_a=280.89$ nm and $\lambda_b=2\lambda_a$, the $Mg(3s^2)+H^+$ channel dominates due to the resonant electronic transition between $X^1\Sigma$ and $A^1\Sigma$ and the detuning Δ_{AB} is always negative.

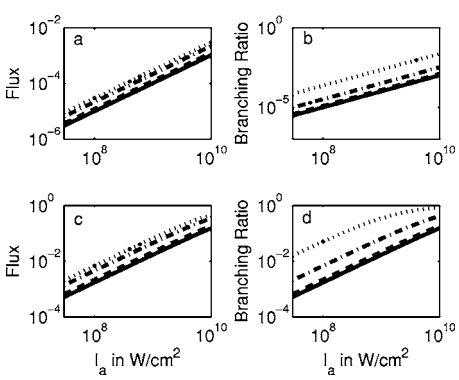

FIG. 8. (a+c) The accumulated flux as a function of the intensity I_b in W/cm^2. (b+d) The branching ratio as a function of the intensity I_b given in W/cm^2. Both x and y axes are log scaled. The following sets of wavelengths have been used $\lambda_a=280.89$ nm and $\lambda_b=2\lambda_a$ for the upper panel (a+b) and $\lambda_a=280.89$ nm and $\lambda_b=620$ nm for the lower panel (c+d). The intensity I_a of the laser field ϵ_a has been varied; 1×10^9 W/cm^2 (solied line), 4×10^9 W/cm^2 (dashed line), 6×10^9 W/cm^2 (dotted-dashed line), and 1×10^{10} W/cm^2 (dotted line).

As the wavelength λ_b increases [cf. Fig. 8(c)] the intensities control the whole range of possible branching ratio. If the intensities $I_a=1\times10^8$ W/cm^2 and $I_b=1\times10^{10}$ W/cm^2, the probability for dissociation is ~0.5 and they would almost selectively dissociate as Mg^++H. The orientation of the transition dipole of the $X^1\Sigma\rightarrow A^1\Sigma$ and $A^1\Sigma\rightarrow C^1\Sigma$ is parallel and $A^1\Sigma\rightarrow B^1\Pi$ is perpendicular. This means that the changing polarization of the ϵ_b field relative to the ϵ_a field is an equivalent control to changing the relative intensities.

V. CONCLUSION AND OUTLOOK

A simulation of a single photodissociation reaction of a cold magnesium hydride ions MgH^+ has been performed with the purpose of exploring the control possibilities. The first step in the modeling of the photodissociation dynamics have been to obtain the adiabatic electronic potential-energy curves. These *ab initio* potential-energy curves were then used for a complete basis set extrapolation. An error less than 3% for the $X^1\Sigma$ and $A^1\Sigma$ potentials was estimated by comparing with spectroscopic values. The accuracy of the two other excited state are not known. These computed potential-energy curves are the basis of the dynamical simulation of the photodissociation process of MgH^+. A control scheme based on varying the frequency and the intensity of each of the laser pulses was studied. It was found that these four control knobs are sufficient to control the branching ratio between the two dissociation channels. It is important to notice that the control of the branching ratio can only be realized if the two laser field are not frequency locked, e.g., $\lambda_b=2\lambda_a$. If two laser fields are frequency locked, $\lambda_b=2\lambda_a$, when the dissociation yield Mg^++H is not observed, only the reaction product $Mg+H^+$ would be detected. The wavelength for the laser field for the electronic transition from $A^1\Sigma$ to $B^1\Pi$ must be around $\lambda_b\sim620$ nm for an enhancement of the yield of the reaction product Mg^++H.

The presented photodissociation model does not include the following processes: spontaneous decay, rotational states, and two-photon electronic transitions.

The lifetime of MgH^+ in the $A^1\Sigma$ electronic state is 4.4 ns, since the time scale for the photodissociation reaction is picosecond the spontaneous decay would not be of importance.

The rotational constant for the lowest vibrational state of the $X^1\Sigma$ is the 6.2 cm^{-1} corresponding to a rotational period of ~2.7 ps. In the current model excited rotational states are not included (only $J=0$), a model which includes transition from specific rovibrational state in the ground electronic state $X^1\Sigma$ to a specific state in the excited electronic state $A^1\Sigma$ obeying the selection rules $\Delta J=\pm1$ is under investigation.

It is possible to couple $X^1\Sigma$ with $C^1\Sigma$ with a two-photon process with laser field ϵ_a. Furthermore, for frequency-locked laser fields two-photon processes with la-

ser field ϵ_b should couple between $X^1\Sigma$ and $A^1\Sigma$ as well as $A^1\Sigma$ and $C^1\Sigma$. This (2+2) photon dissociation channel could interfere with the (1+1) photon dissociation channel. These quantum interferences between the two dissociation pathways for $Mg+H^+$ could be coherently controlled by varying the phase between two laser fields.[2]

The target for the proposed photodissociation scheme is experimentally a sympathetically cooled molecular ion in a Coulomb crystal. The molecular ion can be either in a string of MgH^+ ion sympathetically cooled by the surrounding laser-cooled calcium ions (Ref. 10) or a single molecular ion cooled by a single laser-cooled calcium ion.[6] In both cases the molecular ions are extremely well localized with a distance between them of $\sim 15\ \mu$m, and subsequently the two laser pulses can be focused on the individual molecular ions.

ACKNOWLEDGMENTS

One of the authors (S.J.) is supported by the Carlsberg Foundation. This work was supported by the Israel Science Foundation, DIP Foundation, and the European Research and Training Network *Cold Molecules: Formation, Trapping and Dynamics*. The Fritz Haber Center is supported by the Minerva Gesellschaft für die Forschung, GmbH München, Germany.

[1] S. A. Rice and M. Zhao, *Optical Control of Molecular Dynamics* (Wiley Interscience, New York, 2000).
[2] M. Shapiro and P. Brumer, Rep. Prog. Phys. **66**, 859 (2004).
[3] J. R. Hahn and W. Ho, Phys. Rev. Lett. **87**, 166102 (2001).
[4] S.-W. Hla, L. Bartels, G. Meyer, and K.-H. Rieder, Phys. Rev. Lett. **85**, 2777 (2000).
[5] M. Drewsen, L. Hornekær, N. Kjærgaard, K. Mølhave, A.-M. Thommesen, Z. Videsen, A. Mortensen, and F. Jensen, in *Non-Neutral Plasma Physics IV: Workshop on Non-Neutral Plasmas*, edited by F. Anderegg, L. Schweikhard, and C. F. Driscoll, AIP Conf. Proc. No. 606 (AIP, New York, 2002), p. 1354.
[6] M. Drewsen, A. Mortensen, R. Martinussen, P. Staanum, and J. L. Sørensen, Phys. Rev. Lett. **93**, 243201 (2004).
[7] J. I. Pascual, N. Lorente, Z. Song, H. Conrad, and H.-P. Rust, Nature (London) **423**, 525 (2003).
[8] M. Drewsen, I. S. Jensen, J. Lindballe, N. Nissen, R. Martinussen, A. Mortensen, P. Staanum, and D. Voigt, Int. J. Mass. Spectrom. **229**, 83 (2003).
[9] N. C. Nägerl, D. Leibfried, H. Rohde, G. Thalhammer, J. Eschner, F. Schmidt-Kaler, and R. Blatt, Phys. Rev. A **60**, 145 (1999).
[10] L. Hornekær, N. Kjærgaard, A. M. Thommesen, and M. Drewsen, Phys. Rev. Lett. **86**, 1994 (2001).
[11] A. Bertelsen, I. S. Vogelius, S. Jørgensen, R. Kosloff, and M. Drewsen, Eur. Phys. J. B **31**, 403 (2004).
[12] A. Bertelsen, S. Jørgensen, and M. Drewsen, Phys. Rev. Lett. (submitted); http://arxiv.org/abs/physics/0504128.
[13] I. S. Vogelius, L. B. Madsen, and M. Drewsen, Phys. Rev. Lett. **89**, 173003 (2002).
[14] I. S. Vogelius, L. B. Madsen, and M. Drewsen, J. Phys. B **37**, 4571 (2004).
[15] I. S. Vogelius, L. B. Madsen, and M. Drewsen, Phys. Rev. A **70**, 053412 (2004).
[16] K. Mølhave and M. Drewsen, Phys. Rev. A **62**, 011401 (2000).
[17] W. J. Balfour, Can. J. Phys. **50**, 1082 (1971).
[18] J. M. L. Martin, Chem. Phys. Lett. **259**, 669 (1996).
[19] J. M. L. Martin and P. R. Taylor, Chem. Phys. Lett. **248**, 336 (1996).
[20] A. Halkier, T. Helgaker, P. Jørgensen, W. Klopper, H. Koch, J. Olsen, and A. K. Wilson, Chem. Phys. Lett. **286**, 243 (1998).
[21] D. Feller, J. Chem. Phys. **96**, 6104 (1992).
[22] P. G. Wenthold, Int. J. Mass. Spectrom. **195/196**, 319 (2000).
[23] R. J. Hinde, J. Phys. Chem. A **104**, 7580 (2000).
[24] B. K. Taylor and P. R. Newman, J. Chem. Phys. **118**, 8770 (2003).
[25] B. Paizs, P. Salvador, A. G. Császár, M. Duran, and S. Suhai, J. Comput. Chem. **22**, 196 (2001).
[26] D. Woon and T. Dunning, J. Chem. Phys. **103**, 4572 (1995).
[27] T. Dunning, J. Chem. Phys. **90**, 1007 (1989).
[28] H.-J. Werner and P. J. Knowles, J. Chem. Phys. **82**, 5053 (1985).
[29] P. J. Knowles and H.-J. Werner, Chem. Phys. Lett. **115**, 259 (1985).
[30] H.-J. Werner, P. J. Knowles, R. D. Amos *et al.*, MOLPRO: A package of *ab initio* programs; http://www.molpro.net.
[31] R. Kosloff and H. Tal-Ezer, Chem. Phys. Lett. **127**, 223 (1986).
[32] C. M. Dutta, P. Nordlander, and M. Kimura, Chem. Phys. Lett. **264**, 51 (1997).
[33] T. S. Monteiro, G. Danby, I. L. Cooper, A. S. Dickinson, and E. L. Lewis, J. Phys. B **21**, 4165 (1988).
[34] R. E. Olsen and B. Liu, Phys. Rev. A **20**, 1366 (1979).
[35] R. W. Numrich and D. G. Truhlar, J. Phys. Chem. **79**, 2745 (1975).
[36] R. Kosloff, J. Phys. Chem. **92**, 2087 (1988).
[37] R. Kosloff, Annu. Rev. Phys. Chem. **45**, 145 (1994).
[38] U. V. Riss and H.-D. Meyer, J. Chem. Phys. **105**, 1409 (1996).
[39] A. Vibok and G. G. Balint-Kurti, J. Chem. Phys. **96**, 7615 (1992).
[40] R. Kosloff and D. Kosloff, J. Comput. Phys. **63**, 363 (1986).